

Synthesis of 9-Aminoacridine and its Application as an Anode Material for Aqueous Rechargeable Lithium-ion Batteries

Madhushree M. Ravikumar, Vijeth R. Shetty, Suresh G. Shivappa*

Department of Chemistry and Research Centre, NMKRV College for Women, Jayanagar, Bangalore 560011, Karnataka, India

*Corresponding author: E-mail: sureshssmrv@yahoo.co.in; Tel: (91) 80-22443695; Fax: (91) 80-22440116

Received: 18 December 2018, Revised: 15 February 2019 and Accepted: 19 February 2019

DOI: 10.5185/amlett.2019.9909

www.vbripress.com/aml

Abstract

Two organic compounds namely Acridine (ACD) and 9-aminoacridine (ACD-NH₂) have been investigated as electrode materials for an aqueous rechargeable lithium-ion battery (ARLIB) applications. The electrochemical investigations reveal that the active species act as anodes in ARLIB systems. In this regard, nitrogen group act as redox center and undergo electrochemical reaction with Li-ions during charge and discharge process. The synthesis of 9-aminoacridine is done by standard method called chichibabin reaction. Amination of ACD enhances the electrochemical behaviour of the molecule. To improve the electrochemical performances of ACD & ACD-NH₂, graphene is used as an additive for ARLIB system. The decorated molecules such as decorated Acridine (dACD) and decorated 9-aminoacridine (dACD-NH₂) showed improved electrochemical performance as compared with ACD & ACD-NH₂. The decoration is of great importance concerning capacity, reversibility and stability of cycling behavior during charge and discharge processes. Charge/discharge tests show that ACD, ACD-NH₂, dACD, and dACD-NH₂ have achieved initial discharge capacities of 119, 122, 149 and 220 mAh g⁻¹ respectively at a current density of 0.2 mA. The good cyclic performance and agreeable discharge capacity of the cell signifies the application of dACD-NH₂ as anode material for ARLIB system. Copyright © VBRI Press.

Keywords: Acridine, amino-acridine, graphene, cyclic voltammetry, galvanostatic charge/discharge, electrochemical impedance spectroscopy.

Introduction

Development of novel energy storage devices and renovation methods to overcome the energy associated problems has taken significant trend in modern research. In recent years, rechargeable lithium-ion batteries (RLIBs) have been achieved a great invasion from portable electronics to electrical vehicles due to their high energy density and power density [1-4]. The first detailed description on "rechargeable batteries" was given by Wade in 1902, which was virtually explained the Pb-PbO₂ system. In the mid-1990s, Dahn and his colleagues [5] anticipated a new type of rechargeable Li-ion battery using an aqueous electrolyte to overcome the energy associated problems in RLIBs. The battery technology developed is called aqueous rechargeable lithium ion batteries. Later ARLIB created a tremendous change due to easy availability, cost of active materials and environmental hazardous issues associated with non-aqueous RLIB. In this regard, researchers found their way to develop new types of materials, which are based on eco-friendly concepts and

affordable manufacturing cost. Despite their higher energy density [1, 2], non-aqueous RLIBs suffer from the use of flammable and toxic organic solvents which cause safety problems [3]. Currently, the use of expensive chemicals, technically complex procedures for cell assembly, and high fabrication costs limits their applications in electrochemical energy conversion systems [4]. In aqueous lithium ion batteries, the safety issue was fundamentally established, the conductivity of aqueous solutions is two orders of magnitude higher than that of organic electrolytes and severe manufacturing conditions are ignored, which can accomplish the high rate capacity and specific power. As described by Glanze [6], researchers assumed this development a revolution or big plus because safety drives away and a probable way for the development of a battery system for electric vehicles. The electro activity of electrode material mainly depends on the electrolytic medium such as pH, temperature and types of electrolytic ions involved in electrical conduction. The variation of pH may be due to the generation of H⁺ ions by the electrode material during its electrochemical

performance. This occurs when the fixed potential window, is greater than the degradation potential of water. In principle, materials that are outside the stability range of water will tend to decompose. This is because the positive electrode material that contain lithium and have potentials above the limit of water stability therefore it will react with water and absorbing lithium with the concurrent generation of protons. This will tend to decrease the pH of the water. This conditional abnormality will not happen if the potential window is within the water stability potentials [7]. In spite of above factors, the instability of electrode material in an aqueous medium, also affects the cycling capability of cell. The rapid capacity fading during cycling has been studied by several researchers in aqueous rechargeable lithium-ion battery systems [8]. The initial developments in this field concentrated on the inorganic resources for electrode materials, which assisted with the requirements for superior output [9]. Such inventive approach in the field of energy storage technology is fluctuating in order to obtain the good results from traditional inorganic compounds to new organic substituents.

The usage of organic molecules is one of the criteria to develop them as electrode materials due to their low cost, eco-friendliness, electroactivity etc. [9, 10]. The present lithium ion battery technologies are mainly focusing on the development of environmental friendly green organic electrodes. Organic electrode materials in recent years have also attracted growing attention due to their promising electrochemical performances and distinct advantages in sustainability and environmental friendliness [11]. Furthermore, the unique features of organic materials, such as structure diversity, solubility, flexibility, and processability, make them promising candidates for cathodes or anodes of numerous energy-storage devices [12]. Recently Tarascon and co-workers suggested an advanced step towards the progress of organic electrode materials through an elegant process. They enumerated on conjugated dicarboxylate anodes and lithium salt of tetrahydroxybenzoquinone suggested has a possible alternative to current inorganic based electrodes [13-15]. Latest research on bio-based materials confirmed the prudent use of biomass for value-added chemicals and products in a biorefinery concept [16, 17]. The practice of such low cost, eco-friendly, non-toxic and naturally occurring organic compounds as electrode materials in aqueous rechargeable batteries enhances the applications of LIBs in electric and electronic devices.

The main criterion for noble electroactive species is the availability of active centres for the redox process during electrochemical performance of an organic species. With respect to this, reversible redox properties of carbonyl-based organic molecules have been extensively studied by several groups on few carbonyl compounds such as ellagic acid, purpurin, 5, 7, 12, 14-pentacenetetrone, anthraquinone, dilithium rodizonate,

quinizarin etc. were used as electrode material for RLIBs [18-22]. The molecules containing hydroxyl, amine and carbonyl groups in conjugation with aromatic coordination assist as useful organic electrode materials. The active centres play a major role in the redox process during electrochemical performance [23]. But, organic-based materials have some drawbacks such as low thermal stability, low conductivity, and solubility in organic electrolytes as compared with existing inorganic-based electrode materials [23]. Efforts have been carried out to design new materials with enhanced functionalities resulting in stable reversible redox activities. However, it is extremely inspiring to design organic-based electrodes with high redox potential.

In this regard, for the first time, we proposed a novel organic electrode material called acridine and its derivatives for an aqueous rechargeable lithium ion battery. Acridine and 9-aminoacridine are nitrogen containing heterocyclic compounds. ACD has a similar structure to that of anthracene but has a nitrogen atom in its central ring. The redox processes of Li-ions are influenced by the presence of nitrogen in the molecule. While ACD-NH₂ is a highly fluorescent dye that possesses a solo amino group at the ninth position, which facilitates the tautomeric conformation. In acridine moiety, the carbon-nitrogen double bond group act as redox center and triggers the electron transfer by reversible interaction with lithium ions through the reduction of carbon-nitrogen single bond within the conjugated system and undergoes electrochemical reaction during charge discharge process [24].

However, Acridine moiety exhibits conditions of dissolution and low conductivity which precludes their viability as electrode materials. Thus, to improve the electronic and ionic conductivity of acridine derivatives, the conductive additives are incorporated. Conductive additives play vital role on the electrochemical behavior of active electrode material in LIBs [25]. They create a conductive percolation system to increase and maintain the conductivity persistently during charge-discharge process. In this perspective, allotropy of carbon called graphene was used as conductive additive due to its good electrical conductivity, mechanical strength, high charge mobility and high surface area [26]. Hence, hybrid structures using conducting additives are prepared by incorporating graphene into acridine moiety as a novel electrode material and studied using electrochemical properties like Cyclic Voltammetry (CV), galvanostatic charge/discharge profile (GCPL) and potentiostatic electrochemical impedance spectroscopy (PEIS) techniques.

The electrode materials of acridine moiety shows good stability in the aqueous solution and redox reactions occur within the window of electrochemical stability of water. This behavior is of great importance concerning capacity, reversibility and stability of cycling behavior during charge and discharge

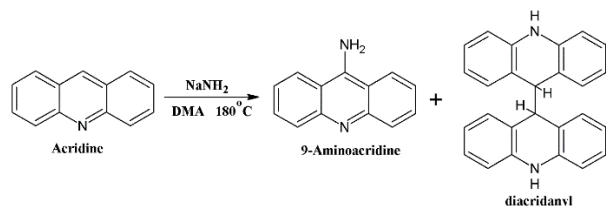
processes. The discharge capacity of the cell is around 83.6 mAh g⁻¹ at C/5 rate has been reported herein. The good cyclic performance and agreeable discharge capacity of the cell signifies the application of acridine and its derivatives as anode material of ARLIBs. Hence acridine seems to be promising electrode material for an aqueous rechargeable lithium ion battery.

In this present work, hybrid structures are prepared by incorporating graphene into organic compounds which can be used as novel electrode materials. In this regard, for the first time, we proposed an organic electrode material called acridine and its derivatives for an aqueous rechargeable lithium-ion battery. The NH₂ group act as redox centers and undergo electrochemical reaction with Li-ions during charge discharge process. The electrode material is stable in the aqueous solution and redox reactions occur within the window of electrochemical stability of water. This behavior is of great importance concerning capacity, reversibility and stability of cycling behavior during charge and discharge processes. The discharge capacity of the cell is around 83.6 mAhg⁻¹ at C/5 rate has been reported herein. The good cyclic performance and agreeable discharge capacity of the cell signifies the application of acridine and its derivatives as anode material of ARLIBs.

Experimental

Chemicals and reagents

Materials and chemicals which were used for our experiments like, acridine, polytetrafluoroethylene powder (12 μmicrons), N-methyl-2-pyrrolidone, and lithium sulfate were purchased from Sigma Aldrich. The physical characterization of the ACD, ACD-NH₂, dACD and dACD-NH₂ was done by SEM (Zeiss Model Supra, Germany) and X-ray powder diffraction studies were made using a XRD Benchtop powder diffraction system using Cu Kα radiation as a source (λ = 0.15443 nm, Proto Manufacturing Inc. Canada). Chemical composition and structure of the compounds were analyzed Bruker 400 MHz processor, Infrared Spectroscopy - FT-IR (PerkinElmer Frontier) studies respectively.



Scheme 1. Acridin-9-amine synthesis.

Scheme for synthesis of acridine derivative

The synthesis of ACD was done by conventional method [27] is as depicted in **Scheme 1**. 9-aminoacridine was obtained by condensation reaction between acridine and sodamide under stirring in

dimethyl aniline as solvent at 180 °C for 3 Hours. The completion of the reaction was monitored by TLC (3:7 EA: Hexane). After the completion of the reaction, the reaction mixture was diluted with known quantity of distilled water. The product separated out from the reaction mixture was filtered and washed with water; a yellow precipitate of crude product was obtained. The obtained crude product was washed with benzene, and again by water to obtain the desired product called acridin-9-amine.

Construction of the cell for electrochemical performance tests

For the cyclic voltammetry studies, a three-electrode electrochemical cell was used. The reference electrode was a saturated calomel electrode and platinum electrode as a counter electrode. The working electrode was the active material which was mechanically immobilized on the surface of the stainless-steel mesh of 1 cm diameter that was held on a steel rod. The working electrode was obtained in the following protocol: 80% active mass, 10% carbon black, and 10% polytetrafluoroethylene binder and the decorated electrodes dACD and dACD-NH₂ were prepared in the stoichiometric ratio of 70% active mass, 10% carbon black, 10% graphene additive and 10% polytetrafluoroethylene binder were mixed well together, and then stirred in N-methyl-2-pyrrolidone for overnight to make a slurry, that applied uniformly on the mesh and then vacuum dried overnight at 85 °C. The loading amount of the active material was ~2 mg cm⁻². All electrochemical measurements were performed in saturated Li₂SO₄ aqueous solutions as the electrolytes. The potential of the electrode was cycled between -1.0 V to 0.5 V with the scan rate ranges 0.1-1.0 mV s⁻¹.

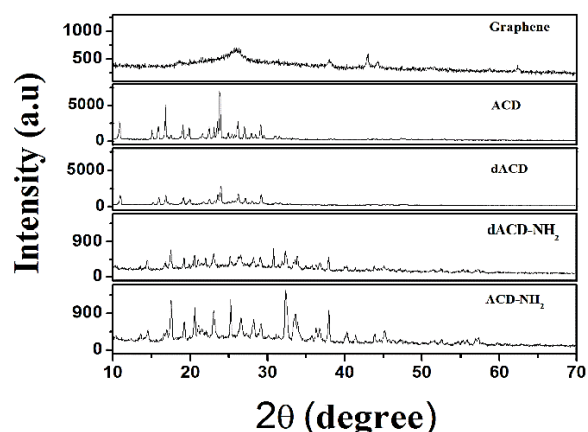


Fig. 1. X-Ray diffraction patterns of acridine, decorated acridine, aminoacridine and decorated aminoacridine.

Results and discussion

Physical characterization

In the present study, acridine and synthesized derivatives were used as working electrodes for ARLIB

systems. The presence of functional groups like amines may proliferates the electrochemical activity which is heading for the battery. In this regard the acridine & ACD-NH₂ were subjected to electrochemical activity vs. SCE. The physical characterizations were carried out by using SEM and pXRD techniques to study the crystallinity and morphological aspects of the molecules respectively. The spectral information was provided by FT-IR, ¹H-NMR techniques.

Powder X-ray diffraction analyses of graphene, acridine, decorated acridine, aminoacridine and decorated 9-aminoacridine were recorded to study their crystalline phase as shown in **Fig. 1**. The XRD profile of graphene shows the 2θ value for graphene at 26.5 [28]. The diffraction peak intensity of the decorated moieties gradually decreases and the line broadening increases as compared to ACD due to the of graphene-carbon group interaction [22].

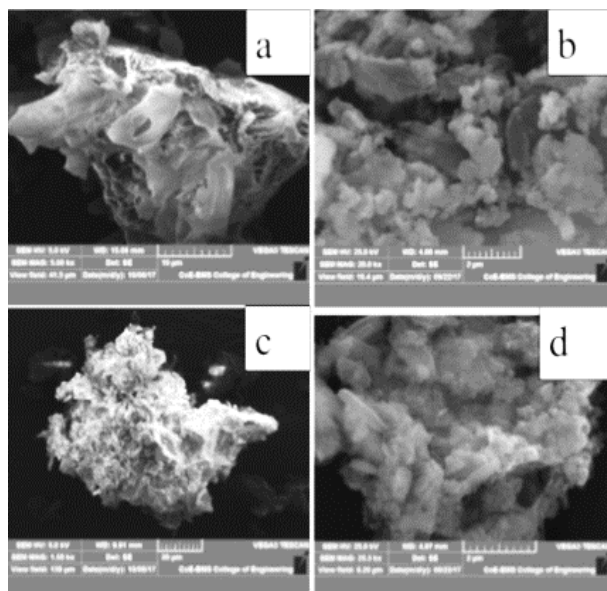


Fig. 2. SEM morphology of (a) Acridine (b) decorated Acridine, (c) Aminoacridine and (d) decorated Aminoacridine.

Scanning electron microscopy studies (**Fig. 2**) displays typical images of acridine and its derivative (a) ACD, (b) dACD, (c) ACD-NH₂ and (d) dACD-NH₂ electrode. **Fig. 2a** and **Fig. 2c** shows the individual ACD and ACD-NH₂ with irregular shape which is distinguished by crystalline particles in the vicinity of 2 μm - 10 μm. As can be observed in **Fig. 2b** and **Fig. 2d**, highly non-homogeneous arrangement of active material and graphene particles as typical sheet morphology. The graphene particles are much larger than those in the composites, suggesting that ACD and ACD-NH₂ may effectively impede the aggregation of the graphene particle [29].

FTIR spectra were carried out in the range of 500 4000 cm⁻¹ and graph designates the distinctive peaks of ACD-NH₂ in **Fig. 3a**.

The broad band in the range of 3431.58cm⁻¹ due to NH₂ stretching group, C=C stretching vibration bands in the range of 2924.23 cm⁻¹, 2853.53cm⁻¹,

1461cm⁻¹ (C-NH₂ stretching + C-H bending), 1595cm⁻¹ (C=C stretching + NH₂ scissoring), 1659.39cm⁻¹ (NH₂scissoring), 1268cm⁻¹ (N-C pyridine stretching + C-H bending).

Overall the presence of the NH₂ group in the ninth position reduces the symmetry and exhibits more bands by stretching the intensity [30].

Fig. 3b demonstrates the ¹H-NMR signals (400 MHz, CDCl₃) for ACD-NH₂. All the aromatic protons of ACD-NH₂ endure a small downfield shift. Therefore, the NMR peaks for the aromatic protons are predicted to suffer similar distinctive multiplet in the range of a 6.68-8.49 ppm and due to the presence of N-H group at the solo position i.e. 9th position shows a significant peak at 8.79 ppm (2H, s) for N-H peak [31].

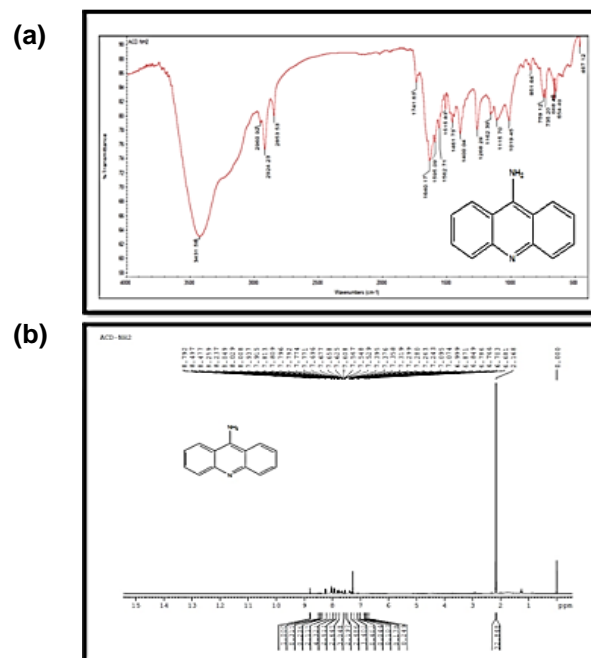


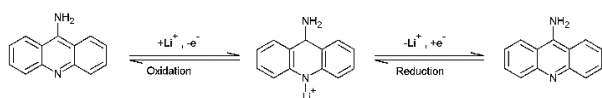
Fig. 3. (a) Infrared spectrum of 9-aminoacridine. (b) ¹H-NMR Spectrum of 9-aminoacridine.

Electrochemical studies

Cyclic voltammetric studies

The cyclic voltammograms of ACD, dACD, ACD-NH₂ and dACD-NH₂ were carried out at room temperature with Platinum as counter electrode and saturated calomel electrode as reference electrode in aqueous solutions containing saturated lithium sulphate. **Fig. 4a** shows the cyclic voltammetry performance of ACD, dACD, ACD-NH₂ and dACD-NH₂ in saturated Li₂SO₄ solution at 0.5 mVs⁻¹. Notably, the redox curves of ACD and ACD-NH₂ intersect at a low potential. It can be seen that the shapes of the CV curves for the four samples are almost similar, indicating that the reduction and oxidation process of the samples are consistent (with the exception of dACD-NH₂). As seen in **Fig. 4a**, ACD shows two pairs of redox peaks at -0.19 V and -0.49 V, which may arise from the formation of a solid electrolyte interface (SEI) layer

[32] and can be assigned to the electrochemical redox process with Li, respectively. However, when graphene is introduced as additive in dACD during the cell preparation, two pairs of redox peaks are obtained at -0.28V and -0.80 V respectively. The decoration to the ACD molecule enhances the peak potential and are attributed to lithiation of dACD and graphene, respectively [33] while coming to ACD-NH₂, two pairs of redox peaks were observed at -0.23 V and -0.52 V respectively. The shifts might be associated with the presence of amine group and formation of tautomeric conformation. In the Fig. 4a, dACD-NH₂ shows high potential redox curves at -0.41 V, 0.11V and -0.87 V, -0.10 V. Among all the molecules, dACD-NH₂ exhibits remarkable results, which is ascribed to lithiation of dACD-NH₂ and presence of graphene [33] as shown in the following Scheme 2.



Scheme 2. Electrode reaction mechanism of anode at three electrode system under 0.5 mV/sec.

These peaks are related to the redox process in electrochemical reaction accompanying gain and loss of electrons in the active sites which reveals the sum of the reductive current is greater than the sum of the oxidative current due to the greater diffusion of the electroactive species under a reductive potential [34]. The electrochemical reaction of dACD-NH₂ attributed to irreversible reduction with solvated lithium ions [35-37] where the first pseudo irreversible anodic peak at -0.85 V, which is ascribed to the occurrence of side reactions on the current collector surface and interfaces due to SEI film formation [36, 37]. According to the literature, the presence of redox peaks in the CV curves is mainly influenced by phase transition phenomenon during the electrochemical performance of the electrode material [38]. The appearance of two pairs of redox peaks signifies disorder transition due to the redox processes in the electrode [39, 40] during lithium transport in aqueous lithium electrolyte. Both the anodic and cathodic peaks are at negative potentials with high reversibility revealing that the active material can be designed to be used as an anode material in ARLIB technology. Depending on the above discussion; we conclude that dACD-NH₂ is stable in aqueous media and can be used as the anode in consideration of its relatively redox potential, low cost and excellent cycling stability in aqueous electrolyte. The hydrogen in the active material enables the site for lithiation during the charging and discharging process as shown in Scheme 2 this was enumerated elsewhere by our group [41].

Based on theoretical view, the potential separation between the peaks and the shape of a specific peak mainly influenced by the size of the particles and applied scan rate [42]. To know the influence of scan rates and peak current on the behaviour of dACD-NH₂

in sat. Li₂SO₄ aqueous electrolyte, cyclic voltammetry studies were performed at increasing the scan rate from 0.1 mV s⁻¹ to 1.0 mV s⁻¹, as shown in the In Fig. 4b, the peak separation in dACD-NH₂ increased with increasing the scan rate and also observed that the anodic and cathodic peaks shift towards more positive and negative potential respectively with increasing the scan rate. The plots of the peak current with the square root of scan rate are as shown in Fig. 4c. It can be seen that, there is a linear relationship among anodic/cathodic peaks with the square root of scan rate. The peak current is proportional to $v^{1/2}$, this can be explained on the basis of scan rate; the redox peaks are well defined at low scan rate than that of medium or high rate due to the diffusion layer configuration which relays on output current and the electrode surface instability is also vital at low scan rates compared to fast scans [43]. Diffusion occurs when there is no complete lithium electron transfer reaction from the electrode which is usually occurs at time interval of a high scan rate. Hence, cyclic voltammetry is used to measure chemical diffusion coefficients of lithium ions. The peak current for a reversible couple can be calculated by the Randles-Sevik equation as given below,

$$i_p = 268,600 n^{1/2} A D^{1/2} C v^{1/2}$$

where, i_p is the peak current, n is the number of electrons involved in charge transfer reaction, A is the area of the electrode in cm², C is the concentration in mol dm⁻³, D is diffusion co-efficient in cm² s⁻¹ and v is the scan rate in mV s⁻¹. The peak current is proportional to $v^{1/2}$, which means that the redox processes occurred is diffusion-controlled process [44].

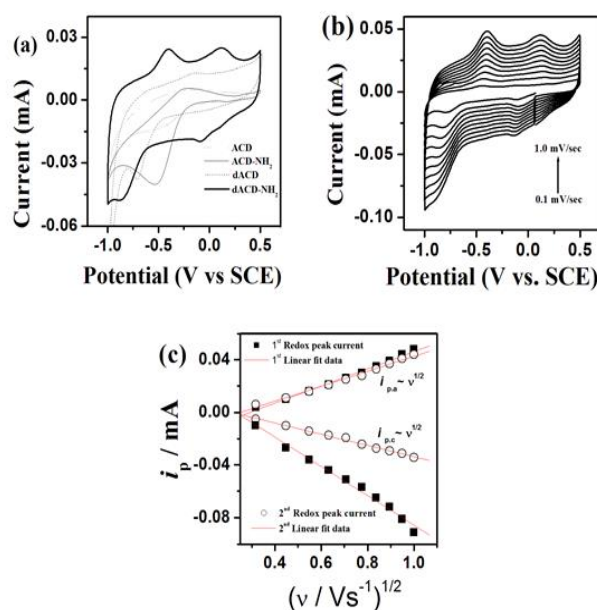


Fig. 4. Cyclic Voltammograms in saturated Li₂SO₄ aqueous electrolyte, (a) Acridine decorated Acridine, Aminoacridine and decorated Aminoacridine scan rate of 0.5 mVs⁻¹, (b) of decorated Aminoacridine at different scan rates to show reversible reaction, (d) Relationship between the peak current density and the square root of scan rate in the cathodic and anodic processes.

Galvanostatic charge/discharge studies

In order to analyze the specific capacity, storage capacity, and cyclability of ACD moieties as electrode material, galvanostatic charge/discharge experiments were carried out within the optimized potential window of the aqueous electrolyte for both half-cell and full cell configuration. **Fig. 5a** shows the comparative charge/discharge studies of ACD, dACD, ACD-NH₂ and dACD-NH₂ moieties at 0.2 mA (C/2) in the potential window of -1.0 to 1.0 mV in three electrode system using sat. Li₂SO₄ as an aqueous electrolyte. To get a closer look at the electrode behavior of the four compounds, charge discharge profiles are plotted. It is clearly seen that the discharge capacity increases in the order ACD (119.16 mAh g⁻¹) < ACD-NH₂ (122.76mAh g⁻¹) < dACD (149.74 mAh g⁻¹) < dACD-NH₂ (220.62mAh g⁻¹). The performance of ACD moieties shows broad redox peaks in aqueous electrolyte which explores a very good reversibility, superior capacity and good rate performance with slight fading. The fade in the capacity may be due to the structural changes of the working electrode during electrochemical cell [45]. Among all the reporting compounds, dACD-NH₂ exhibits a better discharge capacity around 220.62 mAh g⁻¹. These changes in the capacity may be because of graphene incorporation as additive where graphene shows a better electronic conductivity and mechanical properties.

Since the conductive carbon black, graphene and organic binder were homogeneously mixed with the active material and had similar amounts in the modified electrodes, the differences caused by the increase in the conductive agent matters. In this case increasing percentage of conductive material would indeed compensate for increased conductivity of dACD and raise its performance. In this respect, we have fabricated electrodes from ACD and ACD-NH₂ active material with varying percentages conductive material.

The redox process attributed in electrode material during electrochemical reaction can be calculated using the equation.

$$x_{Li^+} = Q \text{ (mA hg}^{-1}\text{)} / T.C$$

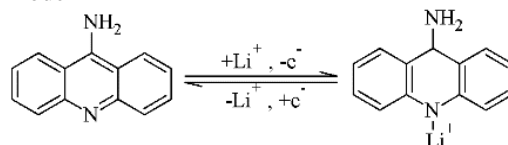
where, x_{Li^+} is the number of Li⁺ electron transfer in the electrode material, Q is discharge capacity and $T.C$ is the theoretical capacity of the electrode material. The equation reveals that existence of partial lithiation is about 1.25 which may due to π - π stacking interaction of the molecules [27]. Hence it proves only one Li⁺ electron transfer reaction may take place with the cathode material.

The cell performance of dACD-NH₂ upto 100 cycles in half cell configuration was performed using sat. Li₂SO₄ electrolyte at 0.08mA (C/5) shown in the **Fig. 5b**. The cell delivers the discharge capacity around 344.7 mAh g⁻¹ at first cycle, 312.2 mAh g⁻¹ at second cycle. This irreversible capacity fading seems to the growth of a solid electrolyte interface (SEI) layer on the surface of the dACD-NH₂ [46]. From the tenth cycle, the cell showed a stable and good reversible capacity of

305.11 mAh g⁻¹ and reached 287.83 mA h g⁻¹ at the 100th cycle. The variation in the capacity may be due to the capacity fade. The capacity fading is mainly because of dissolution effect of the electrode or due to the surface erosion of the material during electrochemical process [47]. The cell dACD-NH₂ exhibits a good reversibility and storage capacity which is greater than that of its theoretical value 138.14 mAh g⁻¹ which clearly shows the aggregation of graphene additive into the dACD-NH₂ also influenced on the increased capacitance [48].

Overall cell performance:

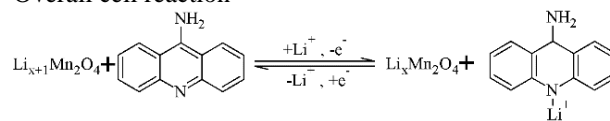
At Anode



At Cathode



Overall cell reaction



Scheme 3. Overall electrode reaction of the cell dACD-NH₂ | aq. saturated Li₂SO₄ | LiMn₂O₄.

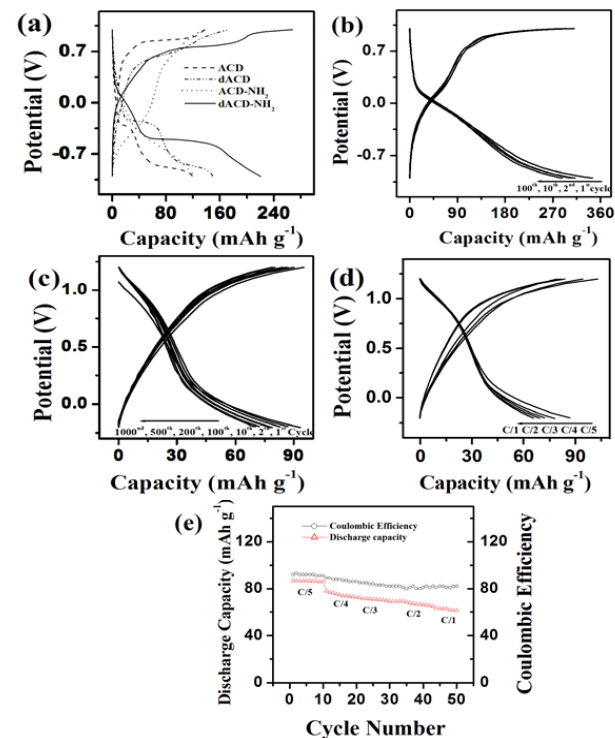


Fig. 5. Galvanostatic charge/discharge measurements in saturated Li₂SO₄ aqueous electrolyte at (a) 3 electrode systems to show the half-cell potential of Acridine decorated Acridine, Aminoacridine and decorated Aminoacridine. (b) The half-cell potential of decorated Aminoacridine upto 100 cycles. (c) dACD-NH₂ | sat. Li₂SO₄ | LiMn₂O₄ cell upto 1000 cycles (d) the cell multiple cycles of dACD-NH₂ | sat. Li₂SO₄ | LiMn₂O₄ at C/5 rate to show rate performance. (e) Discharge capacity and columbic efficiency vs. number of cycles.

Fig. 5c shows the Galvanostatic charge/discharge curves of dACD-NH₂/aq. saturated Li₂SO₄|LiMn₂O₄ composite up to 1000 cycles at C/5 rate. The cell was constructed using dACD-NH₂ as anode and was coupled with cathode LiMn₂O₄. The GCPL studies of dACD-NH₂/aq. saturated Li₂SO₄|LiMn₂O₄ was recorded in an aqueous medium of saturated Li₂SO₄ solution between 1.2 V to -0.2 V potential window. The cell delivers an initial discharge capacity 93.2 mAh g⁻¹ with 92.5% coulombic efficiency, 86.8mAh g⁻¹ with 92.4% coulombic efficiency and 82.91 mA h g⁻¹ with 92.1% at 10th cycle. After 10th cycles, the cell shows a steady decline in the capacity and stabilized after 100th cycle by delivering 78.8 mAh g⁻¹ specific capacity with 93.4% coulombic efficiency. The GCPL profile shows discharge capacity of 78.48 mAh g⁻¹ with 91.62%, 72.30 mAh g⁻¹ with 91.75%, and 70.32 mAh g⁻¹ with 87.68% with respected to the 200th, 500th and 1000th cycles which is as shown in **Table 1**. The curves exhibits a flat discharge plateaus which may be due to the stabilizing effect of the electroactive species [49] or the increase in the polarization of the electrodes or the semi-infinite diffusion of the lithium ion towards the electrodes [22]. The change in the discharge capacity may be because of dissolution effect on the electrode material during electrochemical process or due to crumbling and pulverization of active species influences the discharge capacity fading [55] from 93.2 to 54.5 mA h g⁻¹ from 1st to 1000th cycle respectively.

Table 1. Galvanostatic charge/discharge measurements of dACD-NH₂ | sat. Li₂SO₄ | LiMn₂O₄ cell upto 1000 cycles in saturated Li₂SO₄ aqueous electrolyte

Compound	Potential	Cycle no.	Charge capacity (mA h g ⁻¹)	Discharge capacity (mA h g ⁻¹)
dACD-NH ₂	C/5 rate, 0.05 mA	1	92.10	92.50
		10	92.00	82.91
		100	93.40	78.80
		200	91.62	78.48
		500	91.75	72.30
		1000	87.68	70.32

In order to study the electrode behaviour of dACD-NH₂/aq. saturated Li₂SO₄|LiMn₂O₄ in details, full cell was carried out with different C rates from C/5 to C/1 as shown in the **Fig. 5d**. It shows the rate performance of full-cell battery system at varying current density. The reversible capacity approximately of 86.85mAh g⁻¹ was obtained for C/5 rate and it maintains almost same capacity up to 10 cycles. The increase in the C rates of C/5, C/4, C/3, C/2, and C/1 rates shows the subsequent decrease in capacity of 86.85, 78.5, 72.4, 69.6 and 65.07mAh g⁻¹.

The gradual decrease in the capacity may be due to the formation of solid electrolyte interface [50, 51] on the surface of dACD-NH₂/aq. Saturated Li₂SO₄|LiMn₂O₄ cell. From the figure it is clear that the gradual increase in current densities leads to decrease in the discharge capacity. This clearly shows that the cell

is quite suitable for ARLIBs. **Fig. 5e** shows the discharge capacity and coulombic efficiency at different scan rates of dACD-NH₂ |aq. saturated Li₂SO₄|LiMn₂O₄ cell. From the figure it is clear that the C/5 rate gives the significant discharge capacity at high coulombic efficiency of 92%. By this consideration the graphene moiety as an additive which is an effective material to render the significant electrochemical performance of organic active materials, under appropriate experimental condition. The average cell potential of 0.6 V was obtained by the cell formulation dACD-NH₂ |aq. saturated Li₂SO₄|LiMn₂O₄. The structural manifestation of these materials to be studied further and which will be one of the alternatives for ARLIBs.

Electrochemical impedance spectroscopy studies

Electrochemical impedance spectroscopy (EIS) is an essential technique to determine the kinetic parameters mainly, the chemical diffusion coefficient of lithium ion and to study the lithium ion transfer reaction kinetics. EIS analysis for dACD-NH₂ was carried out and the related Nyquist plots are illustrated in **Fig. 6**. The electrode is cycled for few cycles to make sure the formation of stable surface-electrolyte interface layer on the surface of the electrode before running the EIS. **Fig. 6** shows the Nyquist plot achieved for dACD-NH₂ electrode during redox process in sat Li₂SO₄ aqueous solution respective to the CV peak obtained (**Fig. 4b**). All the Nyquist plots shows three important regions that is high frequency semicircle, middle to low frequency semicircle and a Warburg element in the low frequency region. Migration of lithium ions through the passivating surface layer are observed in the high frequency region, semicircle at high-mid frequency due to parallel combination of charge-transfer resistance (R_{ct}) and double-layer capacitance [52] and a linear region at low frequencies correspond to the diffusion process of Li ions in the electrode. **Fig. 6a** shows the Nyquist plots attained before oxidation potential bias where the semi-circle in the high frequency region and a Warburg lines in the low frequency region are observed. During oxidation potential bias, **Fig. 6b** exhibits the charge transfer resistance in the middle frequency region and Warburg behavior in lower frequency region of the spectra indicating solid state diffusion of lithium ion in the bulk of the electrode [53]. The diameter of the semicircle gradually increases representing the end of charge process shown in the **fig. 6c** similar Nyquist plots are observed during discharge process as shown in **Fig. 6d-f**. The reduction of R_{ct} is due to the lithium insertion process (**Fig. 6d**). The Warburg lines are observed during reduction potential bias (**Fig. 6e**). **Fig. 6f** shows the Nyquist plots obtained after reduction process which indicates the end of redox process.

The values of the parameters calculated from the impedance data during the redox process are showed in **Table 2** and **Table 3**. From the table, it is clearly shows

that the considerable lower R_f values for the organic electrode material which established a better electrical conductivity. The Nyquist plots before oxidation and reduction exhibits semicircle with a R_{ct} Value of 16.12 and 272.15 Ω in the high-middle frequency region respectively, indicates the charge transfer resistance in the electrode material.

Table 2. PEIS Parameters obtained during Charging.

Oxidation				
Sl. No.	Potential in V	R_s in Ω	R_{ct} in Ω	R_f in Ω
Before oxidation				
1	-0.9	34.02	16.12	794.02
2	-0.8	5.0	309.86	3998.6
3	-0.7	4.95	241.71	2809.93
4	-0.6	4.93	4496.83	3576.40
During oxidation				
5	-0.45	4.43	114568.9	0.0763
6	-0.41	4.08	21900	28.99
7	-0.14	3.46	82324.13	0.023
8	-0.11	3.09	17450	23.10
After oxidation				
9	0.2	4.37	189.74	1234.83
10	0.3	3.382	183.46	9805.75
11	0.4	3.352	180.65	8902.03
12	0.5	3.912	206.53	14364.86

Table 3. PEIS Parameters obtained during Discharging.

Reduction				
Sl. No.	Potential in V	R_s in Ω	R_{ct} in Ω	R_f in Ω
Before reduction				
1	0.4	2.998	272.15	86.77
2	0.3	3.197	789.62	88.17
3	0.2	3.669	1255.97	99.32
4	0.1	3.972	970.37	71.79
During reduction				
5	-0.07	4.435	6628.7	415.39
6	-0.74	4.194	3960.39	218.88
7	-0.78	4.943	7341.08	462.97
After reduction				
8	-0.9	5.012	135.15	9802.6
9	-1.0	5.346	137.75	15930.0

During electrochemical reaction, the R_{ct} decreases indicating the activation stage and gradually increases as the reaction approaches the peak potential bias which is ascribed to the morphological changes of active electrode materials and the formation of SEI [54, 55]. As electrochemical reactions proceeds, the SEI layer get stabilized and leads to the viable lithium ion transfer [41] as shown in the EIS plots. The experimental data reveals better electronic conductivity and diffusion of ions during electrochemical process.

During oxidation and reduction render approximately high charge resistance than that of applied potentials due to the presence of active sites in the organic molecules signifies the electro activity of dACD-NH₂ is depended on the change in the structure which effects the electrochemical reaction between active material and the electrolyte, imparting improvements in the electrochemical properties [56].

Fig. 6g shows the equivalent circuit to fit the impedance spectra during the charge process. In this equivalent circuit, R_s symbolize the ohmic resistance of the aqueous media, R_{ct} is the resistance of the charge transfer reaction which is attributed to the diffusion process, R_f is the resistance for Li⁺ movements via surface film interphase, Q is the constant phase element, C_{dl} is the capacitance of the double layer, Z_w is the Warburg impedance.

The respective equivalent circuit is characterized into three parts i.e., (a) the Ohmic resistance in the high frequency region, (b) the R_{ct} and Z_w parallel circuit for the CPE and (c) the R_f parallel circuit for the Q . The frequency-dependent ohmic resistance in the high frequency region is mainly due to the uniform kinetic resistance led to CPE behavior. When the capacitor was replaced by a CPE, the R_{ct} is in series with Z_w and parallel circuit to Q indicates the surface film layer formation on the electrode [57], Z_w and Q form a parallel circuit which is attributed to the Warburg diffusion in the low frequency region. The resistance for lithium migration via surface film interphase is parallel to the Q indicating finite diffusion. This agrees with the outcome of the simulation table of impedance spectra demonstrating the redox process.

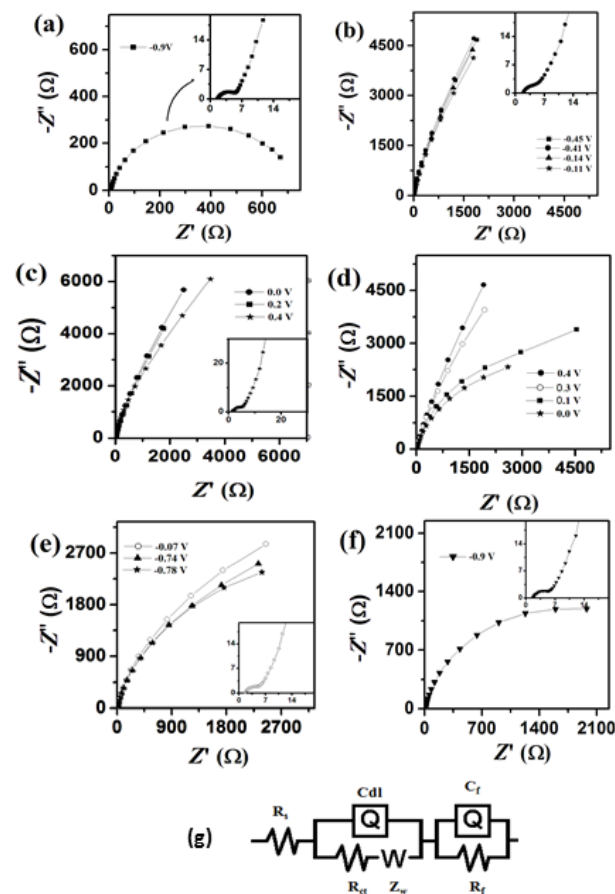


Fig. 6. Nyquist plots to show the impedance response of decorated Aminoacridine anode material at different charge and discharge potential bias (a) before oxidation, (b) during oxidation, (c) after oxidation and (d) before reduction, (e) during reduction, (f) after reduction of electrode material, and (g) equivalent circuit.

Conclusion

In summary, acridine and amino-acridine were developed as an organic electrode material for ARLIB applications. The electrochemical performances of decorated aminoacridine composites showed better output in comparisons with other nitrogen heterocycle and it was influenced firmly by graphene. Incorporation of graphene in the acridine composites exhibited an increase in conductivity & specific capacity and good cyclic stability. The dACD-NH₂ moiety delivered a capacity about 220.62 mAh g⁻¹. The optimized dACD-NH₂/aq. Saturated Li₂SO₄/LiMn₂O₄ cell presented satisfactory electrochemical property and reveals a primary discharge capacity of 93.2 mA h g⁻¹ with 92.5% columbic efficiency capacity retention. The prominent enhancements are due to hybrid structure and improved electron transportation derived from graphene. The results indicated that decorated amino-acridine moieties would be a promising power source for lithium-ion battery applications.

Acknowledgements

The authors gratefully acknowledge the financial support from Vision Group on Science and Technology, Government of Karnataka. We thank Sri A. V. S. Murthy, Honorary Secretary, Rashtreeya Sikshana Samiti Trust, Bangalore and Dr. Snehalata G. Nadiger, Principal, NMKRV College for Women, Bangalore for their continuous support and encouragement.

References

- Armand, M.; Tarascon, J. M.; *Nature*, **2008**, *451*, 652.
- Dunn, B.; Kamath, H.; Tarascon, J. M.; *Science*, **2011**, *334*, 928.
- Chen, J.; Cheng, F.; *Acc. Chem. Res.*, **2009**, *42*, 713.
- Cheng, F.; Liang, J.; Tao, Z.; Chen, J.; *Adv. Mater.*, **2011**, *23*, 1695.
- Wang, X.; Hou, Y.; Zhu, Y.; Wu, Y.; Holze, R.; *Scientific Reports*, **2013**, *3*, 1.
- Wang, G. J.; Yang, L. C.; Qu, Q. T.; Wang, B.; Wu, Y. P.; Holze, R.; *J. Solid State Electrochem.*, **2010**, *14*, 865.
- Ruffo, R.; Wessells, C.; Robert, A. H.; Cui, Y.; *Electrochemistry Communications*, **2009**, *11*, 247.
- Eftekhari, A.; *Electrochim. Acta*, **2001**, *47*, 495.
- Fiksel, J.; *Environmental Science and Technology*, **2003**, *37*, 5330.
- Thomas, R.; Kulkarni, G. U.; *Beilstein Journal of Organic Chemistry*, **2007**, *3*, 1.
- Liang, Y.; Tao, Z.; Chen, J.; *Adv. Energy Mater.*, **2012**, *2*, 742.
- Song, Z.; Zhou, H.; *Energy Environ. Sci.*, **2013**, *6*, 2280.
- Chen, H.; Armand, M.; Demailly, G.; Dolhem, F.; Poizot, P.; Tarascon, J. M.; *Chem. Sus. Chem.*, **2008**, *4*, 348.
- Chen, H.; Armand, M.; Courty, M.; Jiang, M.; Grey, C. P.; Dolhem, F.; Tarascon, J. M.; Poizot, P.; *J. Am. Chem. Soc.*, **2009**, *131*, 8984.
- Armand, M.; Grugeon, S.; Vezin, H.; Laruelle, S.; Ribiere, P.; Poizot, P.; Tarascon, J. M.; *Nat. Mater.*, **2009**, *8*, 120.
- Vemula, P. K.; John, G.; *Acc. Chem. Res.*, **2008**, *41*, 769.
- John, G.; Shankar, B. V.; Jadhav, S. R.; Vemula, P. K.; *Langmuir*, **2010**, *26*, 17843.
- Reddy, A. L. M.; Nagarajan, S.; Chumyim, P.; Gowda, S. R.; Pradhan, P.; Jadhav, S. R.; Dubey, M.; John, G.; Ajayan, P. M.; *Sci. Rep.*, **2012**, *2*, 960.
- Yao, M.; Araki, M.; Senoh, H.; Yamazaki, S.; Sakai, T.; Yasuda, K.; *Chem. Lett.*, **2010**, *39*, 950.
- Fain, V. Y.; Zaitsev, B. E.; Ryabov, M. A.; *Russ. J. Org. Chem.*, **2006**, *42*, 1464.
- Yao, M.; Senoh, H.; Sakai, T.; Kiyobayashi, T.; *Int. J. Electrochem. Sci.*, **2011**, *6*, 2905.
- Vijeth, R. S.; Suresh, G. S.; Ramaiah, M.; Mahadevan, M. K.; Nagaraju, D. H.; *New J. Chem.*, **2015**, *39*, 8534.
- Liang, Y.; Tao, Z.; *Advanced Energy Materials*, **2012**, *2*, 742.
- Chao, Luo.; Xiao, Ji.; Singyuk, Hou.; Nico, Eidson.; Xiulin, Fan.; Yujia, Liang.; Tao, Deng.; Jianjun, Jiang.; Chunsheng, Wang.; *Adv. Mater.*, **2018**, *1706498*, 1.
- Qingtang, Zhang; Zuolong, Yu; Ping, Du; Ce, Su; *Recent Patents on Nanotechnology*, **2010**, *4*, 100.
- Goriparti, S.; Miele, E.; Angelis, F. D.; Fabrizio, E. D.; Zaccaria, R. P.; Capiglia, C.; *Journal of Power Sources*, **2014**, *257*, 421.
- Pozharskii, A. F.; Konstantinchenko, A. A.; *Chemistry of Heterocyclic Compounds*, **1972**, *8*, 1518.
- Mondal, T.; Anil, K.; Bhowmick; Krishnamoorti, R.; *J. Mater. Chem.*, **2012**, *22*, 22481.
- Zhong, L.; Yun, K.; *Int. J. Nanomedicine.*, **2015**, *10*, 79.
- Langhoff S, R.; Charles, W.; Bauschlicher, Jr.; Douglas, M.; Hudgins.; Scott, A.; Sandford.; Louis, J.; Allamandola.; *J. Phys. Chem.*, **1998**, *102*, 1632.
- Sayed, M.; Pal, H.; *Phys. Chem. Chem. Phys.*, **2015**, *17*, 9519.
- Luo, S.; Xu, S.; Zhang, Y.; Liu, J.; Wang, S.; He, P.; *J. Solid State Electrochem.*, **2016**, *20*, 2045.
- Wang, J. Z.; Zhong, C.; Wexler, D.; Idris, N. H.; Wang, Z. X.; Chen, L. Q.; Liu, H. K.; *Chem-Eur J*, **2011**, *17*, 661.
- Kohler, J.; Makihara, H.; Uegaito, H.; Inoue, H.; Toki, M.; *Electrochim. Acta.*, **2000**, *46*, 59.
- Wang, C.; Xu, Y.; Fang, Y.; Zhou, M.; Liang, L.; Singh, S.; Zhao, H.; Schober, A.; Lei, Y.; *J. Am. Chem. Soc.*, **2015**, *137*, 3124.
- Wang, H.; Yuan, S.; Si, Z.; Zhang, X.; *Energy Environ. Sci.*, **2015**, *8*, 3160.
- Zhao, R. R.; Cao, Y. L.; Ai, X. P.; Yang, H. X.; *J. Electroanal. Chem.*, **2013**, *688*, 93.
- Wang, H.; Huang, K.; Zeng, Y.; Zhao, F.; Chen, L.; *Electrochem. Solid-State Lett.*, **2007**, *10*, A199.
- Kim, S. W.; Pyun, S. I.; *Electrochim. Acta*, **2002**, *47*, 2843.
- Nakayama, M.; Ikuta, H.; Uchimoto, Y.; Wakihara, M.; *J. Phys. Chem.*, **2003**, *107*, 10715.
- Vijeth, R. Shetty.; Anil, Kumar.; Gurukara, S. Suresh.; Kittappa, Malavalli, Mahadevan.; *ChemistrySelect*, **2018**, *3*, 8363.
- Levi, M. D.; Aurbach, D.; *J. Electroanal. Chem.*, **1997**, *421*, 79.
- Mi, C. H.; Zhang, X. G.; Li, H. L.; *J. Electroanal Chem.*, **2007**, *602*, 245.
- Wu, M. S.; Wang, M. J.; Jow, J. J.; Yang, W. D.; Hsieh, C. Y.; Tsai, H. M.; *J. Power Sources*, **2008**, *185*, 1420.
- Wang, M.; Yang, M.; Ma, L.; Shen, X.; Zhang, X.; *Journal of Nanomaterials*, **2014**, 368071.
- Wang, W.; Favors, Z.; Ionescu, R.; Ye, R.; Hosseini, Bay, H.; Ozkan, M.; Ozkan, C. S.; *Scientific Reports*, **2015**, *5*, 8781.
- Goriparti, S.; Miele, E.; Angelis, F. D.; Fabrizio, E. D.; Zaccaria, R. P.; Capiglia, C.; *Journal of Power Sources*, **2014**, *257*, 421.
- Zhua, N.; Liub, W.; Xuea, M.; Xiea, Z.; Zhaoa, D.; Zhanga, M.; Chenb, J.; Caoa, T.; *Electrochimica Acta.*, **2010**, *55*, 5813.
- Bu, P.; Liu, S.; Lu, Y.; Zhuang, S.; Wang, H.; Tu, F.; *Int. J. Electrochem. Sci.*, **2012**, *7*, 4617.
- Zhang, M, et al.; *J. Electroanal. Chem.*, **2003**, *559*, 69.
- Xu, C.; Sun, J.; Gao, L.; *Nanoscale*, **2012**, *4*, 5425.
- Sekar, N.; Ramasamy, R. P.; *Journal of Microbial & Biochemical Technology*, **2013**, S6.
- Uwe, Westerhoff.; Kerstin, Kurbach.; Dr., Frank, Lienesch.; Prof. Dr. Michael. Kurrat.; *Energy Technology*, **2016**, *12*, 1620.
- Gupta, S.; Van, M.; Jasinski, J.; *Int. J. Electrochem. Sci.* **2015**, *10*, 10272.
- Goodenough, J. B.; Park, K. S.; *J. Am. Chem. Soc.* **2013**, *4*, 1167.
- Idan, H.; Matthew, D. S.; Pravas, D.; *ACSCatal.*, **2015**, *5*, 6302.
- Leger, C.; Bach, S.; Soudan, P.; Pereira-Ramos, J. P.; *Journal of The Electrochemical Society*, **2005**, *152*, A236.